# Could Fast Radio Bursts Be Standard Candles ?

Han-Yue Guo * and Hao Wei †
*School of Physics, Beijing Institute of Technology, Beijing 100081, China*

**ABSTRACT**

Recently, fast radio bursts (FRBs) have become a thriving field in astronomy and cosmology. Due to their extragalactic and cosmological origin, they are useful to study the cosmic expansion and the intergalactic medium (IGM). In the literature, the dispersion measure DM of FRB has been considered extensively. It could be used as an indirect proxy of the luminosity distance $d_L$ of FRB. The observed DM contains the contributions from the Milky Way (MW), the MW halo, IGM, and the host galaxy. Unfortunately, IGM and the host galaxy of FRB are poorly known to date, and hence the large uncertainties of $\mathrm{DM_{IGM}}$ and $\mathrm{DM_{host}}$ in DM plague the FRB cosmology. Could we avoid DM in studying cosmology? Could we instead consider the luminosity distance $d_L$ directly in the FRB cosmology? We are interested to find a way out for this problem in the present work. From the lessons of calibrating type Ia supernovae (SNIa) or long gamma-ray bursts (GRBs) as standard candles, we consider a universal subclassification scheme for FRBs, and there are some empirical relations for them. In the present work, we propose to calibrate type Ib FRBs as standard candles by using a tight empirical relation without DM. The calibrated type Ib FRBs at high redshifts can be used like SNIa to constrain the cosmological models. We also test the key factors affecting the calibration and the cosmological constraints.

PACS numbers: 98.70.Dk, 98.70.-f, 98.80.Es, 97.10.Vm, 97.10.Bt

* email address: guohanyue7@163.com
† Corresponding author; email address: haowei@bit.edu.cn

## I. INTRODUCTION

Recently, fast radio bursts (FRBs) have become a thriving field in astronomy and cosmology [1–7]. FRBs are millisecond-duration transient radio sources, and their origin is still unknown to date. Most of them are at extragalactic/cosmological distances, as suggested by their large dispersion measures (DMs) well in excess of the Galactic values. Therefore, it is of interest to study cosmology and the intergalactic medium (IGM) with FRBs [1–7].

As is well known, one of the key observational quantities of FRBs is the dispersion measure DM, namely the column density of the free electrons, due to the ionized medium (plasma) along the path. Since the distance along the path in DM records the expansion history of the universe, it plays a key role in the FRB cosmology. The observed DM of FRB at redshift $z$ can be separated into [8–16]

$$\mathrm{DM_{obs}} = \mathrm{DM_{MW}} + \mathrm{DM_{halo}} + \mathrm{DM_{IGM}} + \mathrm{DM_{host}}/(1+z)\,, \tag{1}$$

where $\mathrm{DM_{MW}}$, $\mathrm{DM_{halo}}$, $\mathrm{DM_{IGM}}$, $\mathrm{DM_{host}}$ are the contributions from the Milky Way (MW), the MW halo, IGM, the host galaxy (including interstellar medium of the host galaxy and the near-source plasma), respectively. Obviously, the main contribution to DM of FRB comes from IGM. The mean of $\mathrm{DM_{IGM}}$ is given by [8–16]

$$\langle \mathrm{DM_{IGM}} \rangle = \frac{3cH_0\Omega_b}{8\pi G m_p} \int_0^z \frac{f_{\mathrm{IGM}}(\tilde{z})\, f_e(\tilde{z})\, (1+\tilde{z})\, d\tilde{z}}{h(\tilde{z})}\,, \tag{2}$$

where $c$ is the speed of light, $H_0$ is the Hubble constant, $\Omega_b$ is the present fractional density of baryons, $G$ is the gravitational constant, $m_p$ is the mass of proton, $h(z) \equiv H(z)/H_0$ is the dimensionless Hubble parameter, $f_{\mathrm{IGM}}(z)$ is the fraction of baryon mass in IGM, and $f_e(z)$ is the ionized electron number fraction per baryon. The latter two are functions of redshift $z$ in principle.

One can see that $\langle \mathrm{DM_{IGM}} \rangle$ is related to the expansion history of the universe through $h(z)$ according to Eq. (2). Note that $\langle \mathrm{DM_{IGM}} \rangle$ is the mean value of $\mathrm{DM_{IGM}}$ in all directions of the lines of sight. This is only valid due to the well-known cosmological principle, which assumes that the universe is homogeneous and isotropic on cosmic/large scales. However, it is not homogeneous and isotropic on local/small scales. Thus, $\mathrm{DM_{IGM}} \neq \langle \mathrm{DM_{IGM}} \rangle$ for any observed FRB, since the plasma density fluctuates along the line of sight [17–20] (see also e.g. [8–16]). In the literature, the deviation of $\mathrm{DM_{IGM}}$ from $\langle \mathrm{DM_{IGM}} \rangle$ is usually characterized by the uncertainty $\sigma_{\mathrm{IGM}}(z)$, which is a function of redshift $z$ in principle. Unfortunately, IGM is poorly known in fact. So, one can only consider various empirical $\sigma_{\mathrm{IGM}}(z)$ in the literature, which is usually large ($\sim \mathcal{O}(10^2)$ to $\mathcal{O}(10^3)$ pc cm$^{-3}$) [17–20] (see also e.g. [8–16]). In fact, the large uncertainty $\sigma_{\mathrm{IGM}}(z)$ in $\mathrm{DM_{IGM}}$ is one of the main troubles in the FRB cosmology. On the other hand, $f_{\mathrm{IGM}}(z)$ and $f_e(z)$ in $\langle \mathrm{DM_{IGM}} \rangle$ are both functions of redshift $z$ in principle. Since we are rather ignorant of IGM and the cosmic ionization history, they have been extensively assumed to be constant in the literature. Thus, this also leads to uncertainties in the FRB cosmology.

For convenience, one can introduce the extragalactic DM [8–16], namely

$$\mathrm{DM_E} = \mathrm{DM_{obs}} - \mathrm{DM_{MW}} - \mathrm{DM_{halo}} = \mathrm{DM_{IGM}} + \mathrm{DM_{host}}/(1+z)\,. \tag{3}$$

In the literature, $\mathrm{DM_E}$ has been extensively used to study cosmology. Note that the host galaxy of FRB and hence its contribution to DM are also poorly known. Therefore, $\mathrm{DM_{host}}$ was extensively assumed to be constant in the literature [8–16]. Of course, this simplification prevents us from understanding the cosmic expansion history better.

Although DM is extensively used to study cosmology in the literature, it is just an indirect proxy of the luminosity distance $d_L$ of FRB. In addition, the large uncertainties of $\mathrm{DM_{IGM}}$ and $\mathrm{DM_{host}}$ in DM plague the FRB cosmology, as mentioned above. Could we avoid DM in studying cosmology? Could we instead consider the luminosity distance $d_L$ directly in the FRB cosmology? We are interested to find a way out for this problem in the present work.

Of course, it is difficult to obtain the luminosity distance $d_L$ of FRB. If this FRB is well localized to a host galaxy, and the luminosity distance of this galaxy has been well measured, $d_L$ of this FRB is equal to the one of the host galaxy. Alternatively, if the luminosity distance of objects in the same host galaxy of an FRB (e.g. supernova, gamma-ray burst, or gravitational wave event, not necessarily counterparts)

can be measured, $d_L$ of this FRB is also on hand. But these make sense only at low redshifts. We should find a new method to obtain the luminosity distances $d_L$ for FRBs at high redshifts.

History always repeats itself. As is well known, the distance ladder has been used in many neighboring fields. For example, the luminosity distances of Cepheids can be obtained by using the empirical period versus luminosity ($P-L$, or, Leavitt) relation [21]. If a type Ia supernova (SNIa) shares the same host galaxy with a Cepheid, the luminosity distance of this SNIa is equal to the one of Cepheid. The empirical SNIa light-curve versus luminosity (Phillips) relation [22] could be calibrated by using these SNIa at low redshifts. Thus, the luminosity distances of SNIa at high redshifts can be obtained by extending the calibrated SNIa Phillips relation [23]. Similar to the case of calibrating SNIa as secondary standard candles by using Cepheids as primary standard candles, this has also been considered in the field of gamma-ray bursts (GRBs). The luminosity distances of long GRBs at low redshifts can be obtained by using e.g. interpolation from the ones of SNIa at nearby redshifts [24, 25]. Various empirical relations, especially the $E_{\rm p,\,i}-E_{\rm iso}$ (Amati) relation [26], could be calibrated by using these long GRBs at low redshifts [27] (see also e.g. [24, 25]). Thus, the luminosity distances of long GRBs at high redshifts can be obtained by extending the calibrated GRB empirical relation(s) [24, 25, 28, 29].

The lessons from the above history of calibrating SNIa or long GRBs as standard candles are (a) at least a tight empirical relation involving the luminosity distance is necessary; (b) the empirical relations are only valid for some subclasses, namely SNIa (not for type Ib, Ic and II supernovae), or long GRBs (not for short GRBs). In the present work, we try to calibrate FRBs as standard candles. Thus, we should introduce a universal subclassification scheme for FRBs, and find a tight empirical relation involving the luminosity distance for a subclass of FRBs. Fortunately, they are ready in our previous works.

This paper is organized as followings. In Sec. II, we briefly introduce the universal subclassification scheme and the empirical relations for FRBs. In Sec. III, we describe the method to calibrate type Ib FRBs as standard candles. In Sec. IV, we test the key factors affecting the calibration and the cosmological constraints. In Sec. V, some brief concluding remarks are given.

## II. SUBCLASSIFICATION AND EMPIRICAL RELATIONS FOR FRBS

One of the interesting topics is the classification of FRBs, which is closely related to the origin of FRBs. Clearly, different physical mechanisms are required by different classes of FRBs. Well motivated by the actual observations, they are usually classified into two populations: non-repeating FRBs and repeating FRBs [1–7]. For convenience, we call them type I and II FRBs in [16], respectively.

In the literature, it was speculated for a long time that the FRB distribution tracks the cosmic star formation history (SFH) [1–7]. The well-known Galactic FRB 200428 associated with the young magnetar SGR 1935+2154 [30–33] confirmed that some FRBs originate from young magnetars. On the other hand, some repeating FRBs (such as FRB 121102, FRB 180916.J0158+65, FRB 20190520B, FRB 20181030A) were observed to be closely correlated with star-forming activities [34–37]. Therefore, it is reasonable to expect that at least some (if not all) FRBs are associated with young stellar populations, and hence their distribution tracks SFH. However, this speculation was challenged recently. The newly discovered repeating FRB 20200120E in a globular cluster of the nearby galaxy M81 [38–40] suggested that some FRBs are associated with old stellar populations instead. On the other hand, it was claimed in [41] that the bursts of the first CHIME/FRB catalog [42] as a whole do not track SFH. In [15], it was independently confirmed that the FRB distribution tracking SFH can be rejected at high confidence, and a suppressed evolution (delay) with respect to SFH was found.

The above discussions based on the actual observations have motivated us in [16] to speculate that some FRBs are associated with young populations and hence their distribution tracks SFH, while the other FRBs are associated with old populations and hence their distribution does not track SFH. This led us to propose a universal subclassification scheme for FRBs [16], as shown in Table I.

In [16], we have exercised this subclassification scheme for FRBs by using the actual data of the first CHIME/FRB catalog [42]. These FRBs are subclassified in the transient duration $\nu W$ versus spectral luminosity $L_\nu$ phase plane, with some isothermal lines of brightness temperature $T_B$. The $\nu W-L_\nu$ phase plane has been divided into ten regions by three dividing lines $\nu W=10^{-3}\,{\rm GHz\,s}$, $L_\nu=10^{34}\,{\rm erg/s/Hz}$ and $T_B=2\times10^{35}\,{\rm K}$, which are determined by the minimal p-values of Kolmogorov-Smirnov (KS) test [16]. Note that there are 430 non-repeating (type I) FRBs after the robust cut in the first CHIME/FRB

| **FRBs** | **Class (a) :** associated with old stellar populations | **Class (b) :** associated with young stellar populations |
|---|---|---|
| **Type I :** Non-repeating | **Type Ia :** Non-repeating FRBs associated with old stellar populations and hence delayed with respect to SFH | **Type Ib :** Non-repeating FRBs associated with young stellar populations and hence track SFH |
| **Type II :** Repeating | **Type IIa :** Repeating FRBs associated with old stellar populations and hence delayed with respect to SFH | **Type IIb :** Repeating FRBs associated with young stellar populations and hence track SFH |

TABLE I: A universal subclassification scheme for FRBs proposed in [16].

catalog [42]. Then, we test these 10 regions one by one. For each region, 430 type I FRBs are divided into two samples inside or outside this region. We compare their redshift distributions by using KS test, and also check whether one of these two sample tracks SFH by using the method proposed in [15, 41, 43]. Finally, we find that region (8) is very successful, and hence the physical criteria for the subclassification of type I FRBs have been clearly determined [16], namely

$$\text{Type Ia}: \quad L_\nu \leq 10^{34}\,\text{erg/s/Hz} \quad \& \quad T_B \geq 2\times 10^{35}\,\text{K}\,, \tag{4}$$

$$\text{Type Ib}: \quad \text{otherwise}\,. \tag{5}$$

Note that these physical criteria are suitable for the first CHIME/FRB catalog [42], and they might be changed for the larger and better FRB datasets in the future, but the universal subclassification scheme given in Table I will always hold. We find that in the first CHIME/FRB catalog [42], 65 type Ia FRBs do not track SFH, but 365 type Ib FRBs do track SFH at high confidence. Similarly, we speculate that the possible physical criteria for the subclassification of type II FRBs might be given by [16]

$$\text{Type IIa}: \quad L_\nu \lesssim 10^{29}\,\text{erg/s/Hz} \quad \& \quad T_B \gtrsim 10^{30}\,\text{K}\,, \tag{6}$$

$$\text{Type IIb}: \quad \text{otherwise}\,. \tag{7}$$

We stress that they are highly speculative, because there are only 17 repeaters after the robust cut in the first CHIME/FRB catalog [42], which are too few to form a good enough sample in statistics. Since the data of repeaters will be rapidly accumulated in the future, we hope this subclassification of type II FRBs could be refined. We strongly refer to [16] for the technical details of the subclassification.

In [16], we have found that there are some tight empirical relations for type Ia FRBs but not for type Ib FRBs, and vice versa. These make them different in physical properties. Notice that there are only 17 repeaters after the robust cut in the first CHIME/FRB catalog [42], no empirical relations found for type II FRBs in [16]. On the other hand, there are 65/365 type Ia/Ib FRBs after the robust cut in the first CHIME/FRB catalog [42], respectively. Type Ib FRBs dominate obviously, and hence the empirical relations for them are much tighter than the ones for type Ia FRBs. Unfortunately, the empirical relations only for type Ia FRBs found in [16] do not involve the luminosity distance. In addition, type Ib FRBs are associated with young stellar populations, and hence their distribution tracks SFH. This remarkably facilitates generating the mock type Ib FRBs in simulations. Thus, we choose to only calibrate type Ib FRBs as standard candles in the present work.

Actually, we found some tight empirical relations between spectral luminosity $L_\nu$, isotropic energy $E$ and $\text{DM}_\text{E}$ for type Ib FRBs in [16], where $\text{DM}_\text{E}$ is given by Eq. (3), and

$$L_\nu = 4\pi d_L^2 S_\nu\,, \qquad E = 4\pi d_L^2 \nu_c\, F_\nu/(1+z)\,, \tag{8}$$

in which $d_L$ is the luminosity distance, $S_\nu$ is the flux, $F_\nu$ is the the specific fluence, $\nu_c$ is the central observing frequency ($\nu_c = 600\,\text{MHz}$ for CHIME [42]). The 2-D empirical relations for 365 type Ib FRBs

in the first CHIME/FRB catalog are given by [16]

$$\log E = 0.8862 \log L_\nu + 10.0664 \,, \tag{9}$$

$$\log L_\nu = 2.4707 \log \mathrm{DM_E} + 27.3976 \,, \tag{10}$$

$$\log E = 2.2345 \log \mathrm{DM_E} + 34.2238 \,, \tag{11}$$

where "log" gives the logarithm to base 10, and $E$, $L_\nu$, $\mathrm{DM_E}$ are in units of erg, erg/s/Hz, pc cm$^{-3}$, respectively. In the light of the 2-D empirical relations given by Eqs. (9) – (11), it is anticipated that there is a tight 3-D empirical relation between spectral luminosity $L_\nu$, isotropic energy $E$ and $\mathrm{DM_E}$. Fitting to the data, we also found this 3-D empirical relation in [16] for 365 type Ib FRBs in the first CHIME/FRB catalog, namely

$$\log L_\nu = 1.1330 \log \mathrm{DM_E} + 0.5986 \log E + 6.9098 \,. \tag{12}$$

Noting that the empirical relations in Eqs. (10) – (12) involve $\mathrm{DM_E}$, they are not suitable for our goal, as mentioned in Sec. I. Fortunately, the empirical relation in Eq. (9) does not involve DM, but it does involve the luminosity distance $d_L$ (n.b. Eq. (8)), and hence it works well for calibrating type Ib FRBs as standard candles. We strongly refer to [16] for the technical details of the empirical relations.

## III. CALIBRATING TYPE IB FRBS AS STANDARD CANDLES

It is worth noting that the above empirical relations were found by using the first CHIME/FRB catalog [42], and the values of slopes and intercepts might be changed for the larger and better FRB datasets in the future. So, one should not persist in their numerical values. The key point is that these empirical relations do exist in such forms for type Ib FRBs.

Here, we assume that the empirical $L_\nu - E$ relation really exists due to the unknown physical mechanism for the engines of type Ib FRBs. It takes the form of Eq. (9), namely

$$\log \frac{E}{\mathrm{erg}} = a \log \frac{L_\nu}{\mathrm{erg/s/Hz}} + b \,, \tag{13}$$

where $a$ and $b$ are both dimensionless constants. In particular, $a = 0.8862$ and $b = 10.0664$ [16] for 365 type Ib FRBs in the first CHIME/FRB catalog. Note that the luminosity distance $d_L$ is implicit in the empirical $L_\nu - E$ relation given by Eq. (13). Using Eq. (8), we recast Eq. (13) as

$$\mu = -\frac{5}{2\,(1-\alpha)} \log \frac{F_\nu/(1+z)}{\mathrm{Jy\ ms}} + \frac{5\alpha}{2\,(1-\alpha)} \log \frac{S_\nu}{\mathrm{Jy}} + \beta \,, \tag{14}$$

where $\alpha = a \neq 1$, $\beta =$ const. is a complicated combination of $a$, $b$, $\nu_c$/MHz, and $\mu$ is the well-known distance modulus defined by

$$\mu = 5 \log \frac{d_L}{\mathrm{Mpc}} + 25 \,. \tag{15}$$

Unlike $L_\nu$ and $E$ in Eq. (13), we note that $F_\nu$, $S_\nu$ and $\mu$ (equivalently $d_L$) are all observed quantities, and hence it is more convenient to instead use Eq. (14) in calibrating type Ib FRBs as standard candles. There are two free parameters $\alpha$ and $\beta$ in Eq. (14), and they will be calibrated by using type Ib FRBs at low redshifts.

Of course, current data of FRBs are certainly not enough to calibrate type Ib FRBs as standard candles. So, it will be a proof of concept by using the simulated FRBs in the present work. We assume that there will be a large amount of type Ib FRBs with identified redshifts in the future. If a non-repeating (type I) FRB has been precisely localized by using e.g. VLBI down to the milliarcsecond level [44, 45] or better in the future, its host galaxy and local environment can be well determined. Subsequently, it is a type Ib FRB if this FRB lives in a star-forming environment. Its redshift could be identified by using the spectrum of the host galaxy.

On the other hand, the luminosity distance $d_L$ (equivalently the distance modulus $\mu$) of type Ib FRBs should be independently measured to build the Hubble diagram. This is a fairly difficult task at high redshifts. But it is possible to measure the luminosity distance of type Ib FRBs at enough low redshifts. Fortunately, the redshift range of FRBs is very wide. They could be at very high redshifts $z > 3$ (even $z \sim 15$ [46]), and hence they might be a powerful probe for the early universe. On the other hand, they can also be at very low redshifts, even in our Milky Way ($z = 0$) as shown by the Galactic FRB 200428. In fact, many nearby FRBs at very low identified redshifts were found [47]. Thus, it is possible that a type Ib FRB and a SNIa or a Cepheid are in the same host galaxy, and hence the luminosity distance $d_L$ (equivalently the distance modulus $\mu$) of type Ib FRB is equal to the one of SNIa or Cepheid. Note that type Ib FRB and SNIa/Cepheid are not necessarily associated. This is just similar to the case of calibrating SNIa as standard candles by using Cepheids, as mentioned in Sec. I. Because Cepheids are certainly at very low redshifts and SNIa can be at not so low redshifts (for example, $z \sim 0.1$ or 0.5), we only consider the case of SNIa in this work. As is well known, currently the distance modulus $\mu$ of SNIa can be measured very precisely. It is also expected that the precision will be significantly improved in the future. Thus, it is reasonable to assume that the distance modulus $\mu$ of type Ib FRB at low redshifts could also be measured in the future with the precision comparable with the one of SNIa.

If the number of type Ib FRBs at low redshifts with measured distance moduli $\mu$, redshifts $z$, fluence $F_\nu$ and flux $S_\nu$ is large enough, the empirical relation in Eq. (14) could be well calibrated by fitting it to these type Ib FRBs. In this way, the free parameters $\alpha$ and $\beta$ in Eq. (14) and their uncertainties will be determined. Then, we assume this calibrated empirical relation in Eq. (14) is universal, namely it also holds at high redshifts. Now, for each type Ib FRB at high redshift, its redshifts $z$, fluence $F_\nu$ and flux $S_\nu$ has been observed, and the parameters $\alpha$, $\beta$ take the same values determined at low redshift in the previous step. Consequently, its distance modulus $\mu$ (equivalently the luminosity distance $d_L$) in the left hand side of Eq. (14) can be derived since the quantities in the right hand side of Eq. (14) are all known now. Its error $\sigma_\mu$ can also be obtained by using the error propagation. So, the Hubble diagram of type Ib FRBs at high redshifts is on hand. We can use these type Ib FRBs with known distance moduli $\mu$, errors $\sigma_\mu$, and redshifts $z$ to constrain the cosmological models, similar to the case of SNIa.

## IV. KEY FACTORS AFFECTING THE CALIBRATION AND THE COSMOLOGICAL CONSTRAINTS

As mentioned above, current data of FRBs are not enough to calibrate type Ib FRBs as standard candles. Thus, we have to use the mock type Ib FRBs instead. But the same pipeline holds for the actual type Ib FRBs in the future. In the followings, we briefly describe how to generate the mock type Ib FRBs, and calibrate type Ib FRBs as standard candles. Then, we use the calibrated type Ib FRBs at hight redshifts to constrain the cosmological model. Clearly, there are many key factors affecting the calibration and the cosmological constraints. We will test them one by one.

### A. Generating the mock type Ib FRBs

Here, we generate the mock type Ib FRBs closely following the method used in [15, 16] (see also [41]), but the distribution of type Ib FRBs should track SFH. The mock observed type Ib FRB redshift rate distribution is given by [15, 16, 41]

$$\frac{dN}{dt_{\rm obs}\, dz} = \frac{1}{1+z} \cdot \frac{dN}{dt\, dV} \cdot \frac{c}{H_0} \cdot \frac{4\pi d_C^2}{h(z)}\,, \tag{16}$$

where the comoving distance $d_C = d_L/(1+z)$, and $dt/dt_{\rm obs} = (1+z)^{-1}$ due to the cosmic expansion is used. In the present work, we consider the flat $\Lambda$CDM cosmology, and hence the dimensionless Hubble parameter $h(z)$ and the luminosity distance $d_L$ read

$$h(z) \equiv H(z)/H_0 = \left[\, \Omega_m \,(1+z)^3 + (1-\Omega_m) \,\right]^{1/2}\,, \qquad d_L = \frac{c}{H_0}\,(1+z) \int_0^z \frac{d\tilde{z}}{h(\tilde{z})}\,. \tag{17}$$

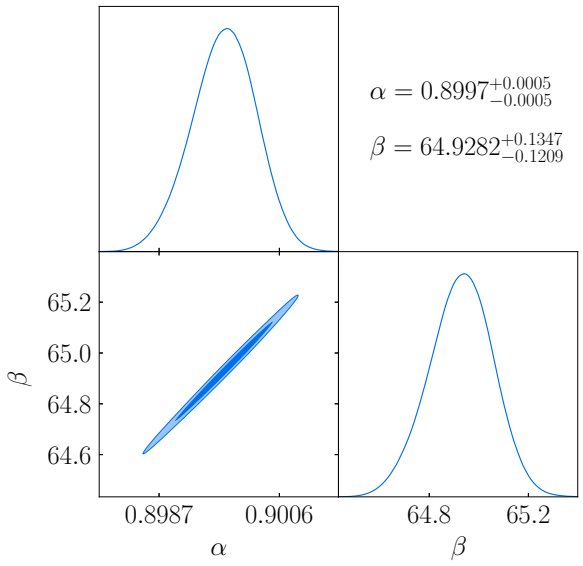


FIG. 1: The marginalized $1\sigma$ constraints on the parameters $\alpha$, $\beta$ in the empirical relation (14) and their contours from the data of type Ib FRBs at low redshifts $z < z_d$ for the fiducial case. See Sec. IV B for details.

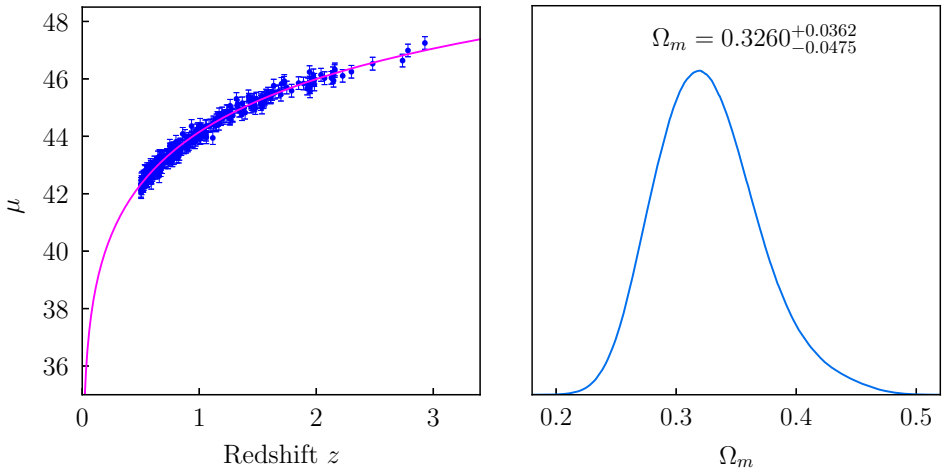


FIG. 2: Left panel: The Hubble diagram $\mu$ versus $z$ for type Ib FRBs at high redshifts $z \geq z_d$. The magenta line indicates the flat ΛCDM cosmology with the best-fit $\Omega_m$ given in the right panel. Right panel: The marginalized $1\sigma$ constraint on the parameter $\Omega_m$ in the flat ΛCDM cosmology from the data of type Ib FRBs at high redshifts $z \geq z_d$. Note that they are both for the fiducial case. See Sec. IV B for details.

Here, we adopt $\Omega_m = 0.3153$ and $H_0 = 67.36\,\mathrm{km/s/Mpc}$ from the Planck 2018 results [48]. Since the intrinsic type Ib FRB redshift distribution tracks SFH, we have $dN/(dt\,dV) \propto \mathrm{SFH}(z)$, while the latest result from the observations for SFH is given by [49] (see also [15, 16])

$$\mathrm{SFH}(z) \propto \frac{(1+z)^{2.6}}{1+((1+z)/3.2)^{6.2}}\,. \tag{18}$$

On the other hand, we generate the isotropic energy $E$ for the mock type Ib FRBs with [15, 16, 41]

$$dN/dE \propto (E/E_c)^{-s} \exp\left(-E/E_c\right)\,, \tag{19}$$

where we adopt $s = 1.9$ and $\log\left(E_c/\mathrm{erg}\right) = 41$, well consistent with the observations [15, 16]. We generate $N_{\mathrm{sim}}$ mock type Ib FRBs as follows: (i) for each mock type Ib FRB, randomly assign a mock redshift $z$

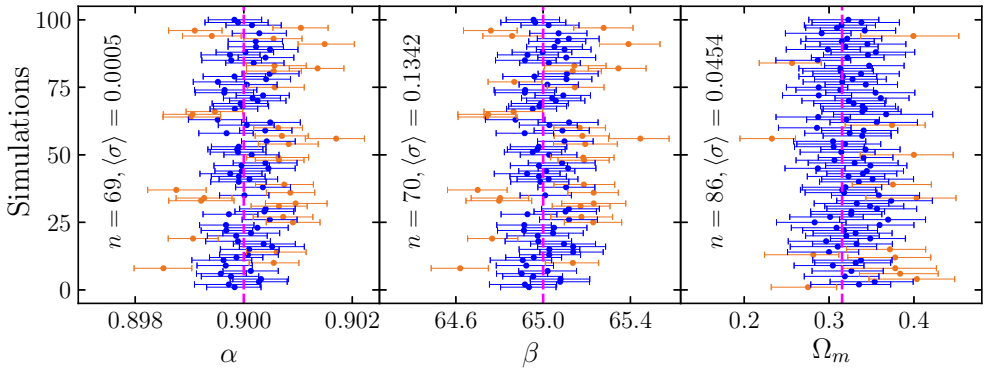


FIG. 3: The marginalized $1\sigma$ constraints on the parameters $\alpha$ (left panel), $\beta$ (middle panel) in the empirical relation (14) and the cosmological parameter $\Omega_m$ (right panel) for 100 simulations in the fiducial case. The blue means with error bars (the chocolate means with error bars) indicate that the assumed $\alpha = 0.9$, $\beta = 65$ or $\Omega_m = 0.3153$ (indicated by the magenta dashed lines) are consistent (inconsistent) with the mock type Ib FRBs within $1\sigma$ region, respectively. In each panel, $n$ and $100 - n$ are the numbers of blue and chocolate means with error bars, respectively. $\langle\sigma\rangle$ is the mean of the uncertainties of 100 constraints on the parameters $\alpha$ (left panel), $\beta$ (middle panel) and $\Omega_m$ (right panel). See Sec. IV B for details.

to this FRB from the redshift distribution in Eq. (16); (ii) generate a mock energy $E_{\rm int}$ randomly from the distribution in Eq. (19) for this FRB; (iii) derive the luminosity distance $d_{L,\,\rm int}$ and the distance modulus $\mu_{\rm int}$ by using Eqs. (17) and (15) with the mock redshift $z$ for this FRB; (iv) derive the fluence $F_{\nu,\,\rm int}$ by using Eq. (8) with $E_{\rm int}$, $d_{L,\,\rm int}$, $\nu_c = 600\,\rm MHz$ (the one of CHIME [42]) and the mock redshift $z$ for this FRB; (v) assign an error $\sigma_{F,\,\rm obs} = \sigma_{F,\,\rm rel}\,F_{\nu,\,\rm int}$ to the "observed" flence $F_{\nu,\,\rm obs}$ for this FRB, while $F_{\nu,\,\rm obs}$ is randomly assigned from a Gaussian distribution with the mean $F_{\nu,\,\rm int}$ and the standard deviation $\sigma_{F,\,\rm obs}$. Note that the relative error $\sigma_{F,\,\rm rel}$ will be specified below; (vi) repeat the above steps for $N_{\rm sim}$ times. Finally, $N_{\rm sim}$ mock type Ib FRBs are on hand.

But these $N_{\rm sim}$ mock type Ib FRBs intrinsically generated above are not the ones "detected" by the telescope, due to the telescope's sensitivity threshold and instrumental selection effects near the threshold. So, the next step is to filter them by using the telescope's sensitivity model, which is chosen to be the one for CHIME considered in [15, 16, 41]. The sensitivity threshold is $\log F_{\nu,\,\rm min} = -0.5$ for CHIME, where the specific fluence is in units of Jy ms. The FRBs with fluences below this threshold cannot be detected. On the other hand, there is a "gray zone" in the $\log F_\nu$ distribution, within which CHIME has not reached full sensitivity to all sources, due to the direction-dependent sensitivity of the telescope [15, 16, 41]. The detection efficiency parameter in the "gray zone" is given by $\eta_{\rm det} = \mathcal{R}^3$, where $\mathcal{R} = (\log F_{\nu,\,\rm th} - \log F^{\rm min}_{\nu,\,\rm th})/(\log F^{\rm max}_{\nu,\,\rm th} - \log F^{\rm min}_{\nu,\,\rm th})$, such that $\eta_{\rm det} \to 0$ at $\log F^{\rm min}_{\nu,\,\rm th} = -0.5$ and $\eta_{\rm det} \to 1$ at $\log F^{\rm max}_{\nu,\,\rm th}$. Outside the "gray zone", $\eta_{\rm det} = 1$. For type Ib FRBs tracking SFH, we set $\log F^{\rm max}_{\nu,\,\rm th} = 0.9$, which is very close to the best value found in Table II of [16].

In the present work, we generate a pool of mock type Ib FRBs "detected" by the telescope to save the computational power and time. That is, we randomly generate $N_{\rm sim} = 500,000,000$ mock type Ib FRBs, and then filter them by using the telescope's sensitivity model, as mentioned above. Finally, about 40,000 mock "detected" type Ib FRBs after the filter enter this pool. When $N_{\rm FRB}$ mock type Ib FRBs are needed in the following subsections, we randomly sample them from this pool.

The next step is to assign the mock flux and its error for each mock type Ib FRB in this pool. We assume that the underlying empirical relation in Eq. (14) is acutally

$$\mu = -25\log\frac{F_\nu/(1+z)}{\rm Jy\ ms} + 22.5\log\frac{S_\nu}{\rm Jy} + 65\,, \tag{20}$$

which corresponds to $\alpha = 0.9$ and $\beta = 65$, or equivalently $a = 0.9$ and $b \simeq 10.1$ approximately in Eq. (13). We can derive $S_{\nu,\,\rm int}$ by using Eq. (20) with $\mu_{\rm int}$, $F_{\nu,\,\rm int}$ and the mock redshift $z$ for this FRB. We assign an error $\sigma_{S,\,\rm obs} = \sigma_{S,\,\rm rel}\,S_{\nu,\,\rm int}$ to the "observed" flux $S_{\nu,\,\rm obs}$ for this FRB, while $S_{\nu,\,\rm obs}$ is randomly assigned from a Gaussian distribution with the mean $S_{\nu,\,\rm int}$ and the standard deviation $\sigma_{S,\,\rm obs}$. Similarly, we assign an error $\sigma_{\mu,\,\rm obs} = \sigma_{\mu,\,\rm rel}\,\mu_{\rm int}$ to the "observed" distance modulus $\mu_{\rm obs}$ for this FRB, while $\mu_{\rm obs}$ is randomly assigned from a Gaussian distribution with the mean $\mu_{\rm int}$ and the standard deviation $\sigma_{\mu,\,\rm obs}$. Note that the relative errors $\sigma_{S,\,\rm rel}$ and $\sigma_{\mu,\,\rm rel}$ will be specified below.

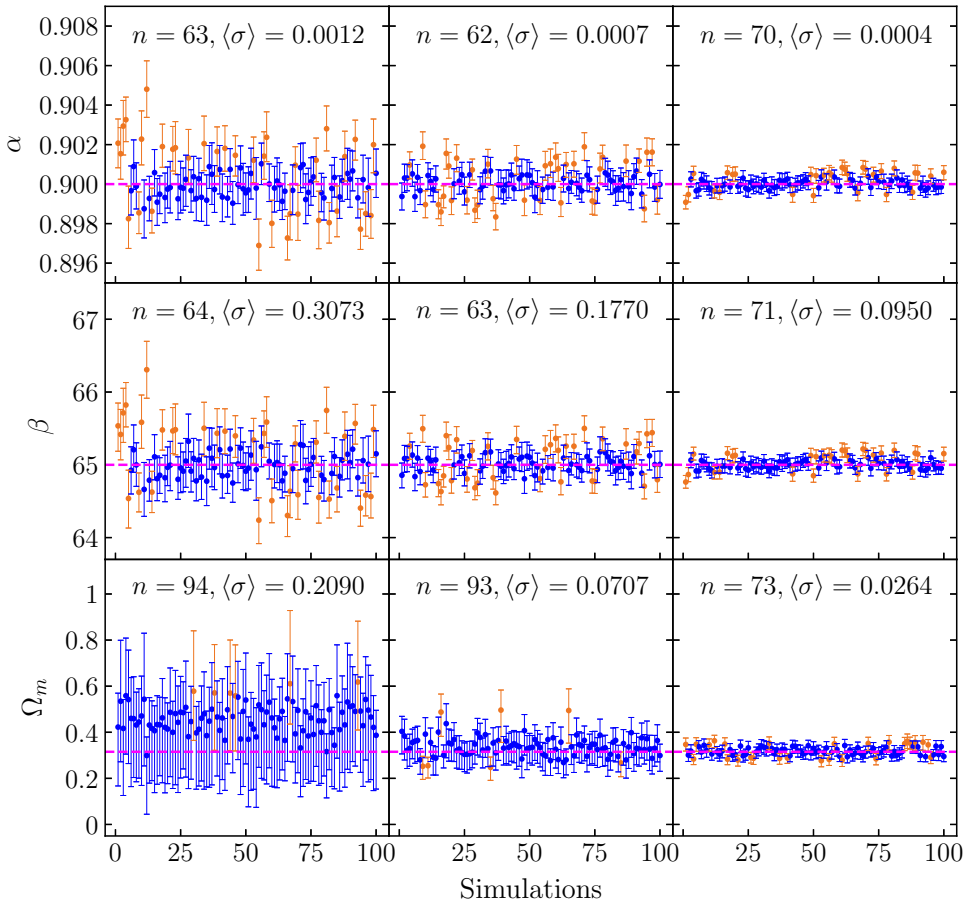


FIG. 4: The same as in Fig. 3, but for the cases of $N_{\rm FRB} = 100$ (left panels), 300 (middle panels) and 1000 (right panels) type Ib FRBs, respectively. Fig. 3 ($N_{\rm FRB} = 500$) should be viewed together. See Sec. IV C for details.

So far, a pool of about 40,000 mock "detected" type Ib FRBs with the "observed" redshifts $z$, fluences $F_{\nu,\,\rm obs}$ and their errors $\sigma_{F,\,\rm obs}$, fluxes $S_{\nu,\,\rm obs}$ and their errors $\sigma_{S,\,\rm obs}$, are ready. In addition, the "observed" distance moduli $\mu_{\rm obs}$ and their errors $\sigma_{\mu,\,\rm obs}$ for the mock type Ib FRBs at low redshits are also on hand. We will pretend to use them as the actual ones blindly in the followings.

### B. The fiducial case

At first, we consider the fiducial case, and the other cases below will be compared with it. In this fiducial case, we consider $N_{\rm FRB} = 500$ mock type Ib FRBs, which can be randomly sampled from the pool built in Sec. IV A. On the other hand, although the fluence and flux of FRBs cannot be measured with high precision currently by the telescope (e.g. CHIME), we assume that they could be measured precisely in the future. So, in the fiducial case, we set the relative errors $\sigma_{F,\,\rm rel}$ and $\sigma_{S,\,\rm rel}$ to be both 1%. As mentioned above, we obtain the distance modulus of type Ib FRB at low redshift by equaling it to the one of SNIa in the same host galaxy. As is well known, currently the distance modulus $\mu$ of SNIa can be measured very precisely. It is expected that the precision will be significantly improved in the future. For example, the expected aggregate precision of SNIa detected by the Roman Space Telescope (formerly WFIRST, planned for launch in the mid-2020s) is 0.2% at $z < 1$ [50]. So, in the fiducial case, we set the relative error $\sigma_{\mu,\,\rm rel} = 0.2\%$ for type Ib FRBs at low redshifts. Of course, we need a redshift divide $z_d$ to define "low" ($z < z_d$) and "high" ($z \geq z_d$) redshifts. In the fiducial case, we set $z_d = 0.5$.

Following the instructions in Sec. III, we calibrate the empirical relation (14) by using type Ib FRBs at low redshifts $z < z_d$. To this end, we use the Markov Chain Monte Carlo (MCMC) code Cobaya [51], which is the Python version of the well-known CosmoMC [52]. Fitting the empirical relation given by

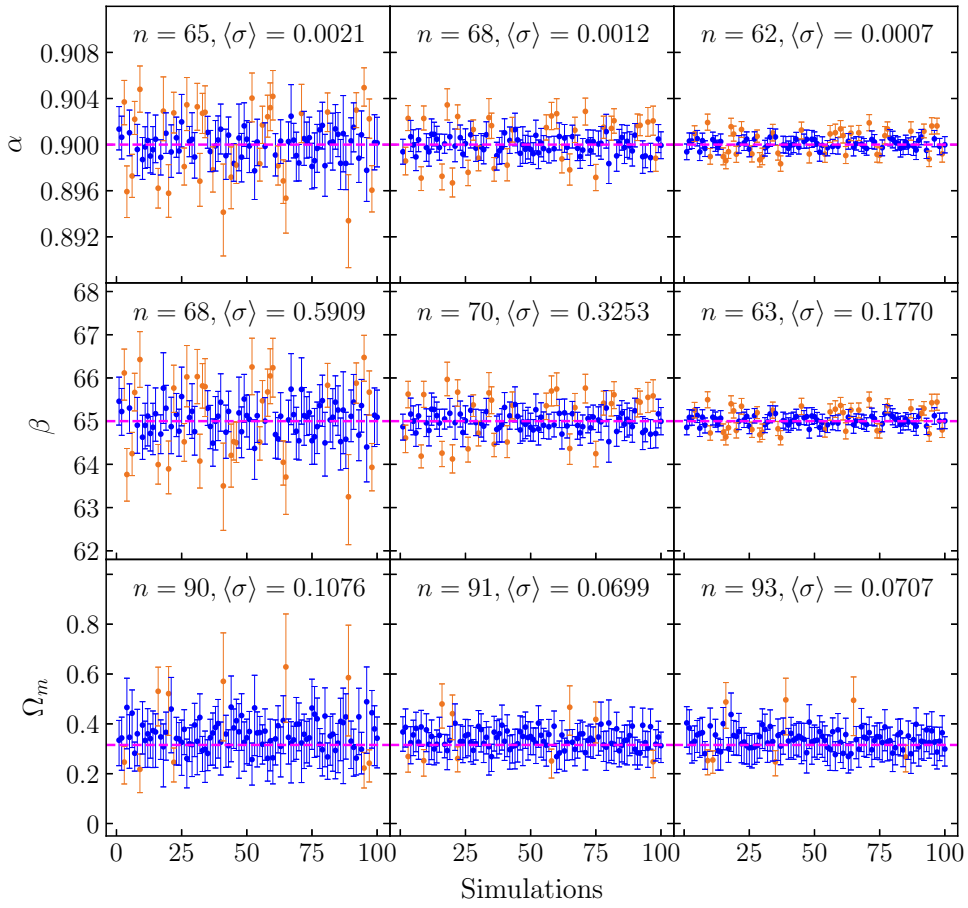


FIG. 5: The same as in Fig. 3, but for the cases of $N_{\rm FRB} = 300$ and $z_d = 0.1$ (left panels), 0.2 (middle panels) and 0.5 (right panels) type Ib FRBs, respectively. See Sec. IV D for details.

Eq. (14) to the data of type Ib FRBs at low redshifts $z < z_d$, we find the marginalized $1\sigma$ constraints on the parameters $\alpha$ and $\beta$, namely

$$\alpha = 0.8997^{+0.0005}_{+0.0005}\,, \qquad \beta = 64.9282^{+0.1347}_{-0.1209}\,, \tag{21}$$

and we also present the contours and the marginalized probability in Fig. 1. Then, assuming the calibrated empirical relation (14) with $\alpha$ and $\beta$ given in Eq. (21) still holds at high redshifts $z \geq z_d$, we can derive the distance moduli $\mu$ for type Ib FRBs at high redshifts $z \geq z_d$ with their observed flences $F_{\nu,\,\rm obs}$ and fluxes $S_{\nu,\,\rm obs}$. Their errors $\sigma_\mu$ can also be obtained by using the error propagation. In the left panel of Fig. 2, we present the Hubble diagram $\mu$ versus $z$ for type Ib FRBs at high redshifts $z \geq z_d$, while the error bars $\sigma_\mu$ are also plotted. Fitting the flat $\Lambda$CDM cosmology given by Eq. (17) to the distance moduli $\mu(z_i)$ data of type Ib FRBs at high redshifts $z \geq z_d$, we obtain the $1\sigma$ constraint on $\Omega_m$, namely

$$\Omega_m = 0.3260^{+0.0362}_{-0.0475}\,, \tag{22}$$

while the Hubble constant $H_0$ has been marginalized. We also present the marginalized probability in the right panel of Fig. 2. Clearly, the assumed value $\Omega_m = 0.3153$ used in Sec. IV A to generate the mock type Ib FRBs is well consistent with the one in Eq. (22).

To avoid the statistical noise due to random fluctuations, one should repeat the above constraints for a large number of simulations. But it is expensive to consider too many simulations since they consume a large amount of computation power and time. As a balance, here we consider 100 simulations, which is enough in fact. In Fig. 3, we present the marginalized $1\sigma$ constraints on the parameters $\alpha$, $\beta$ in the empirical relation (14) and the cosmological parameter $\Omega_m$ for 100 simulations in the fiducial case. It is easy to see from Fig. 3 that the assumed values $\alpha = 0.9$, $\beta = 65$, and $\Omega_m = 0.3153$ used in Sec. IV A to

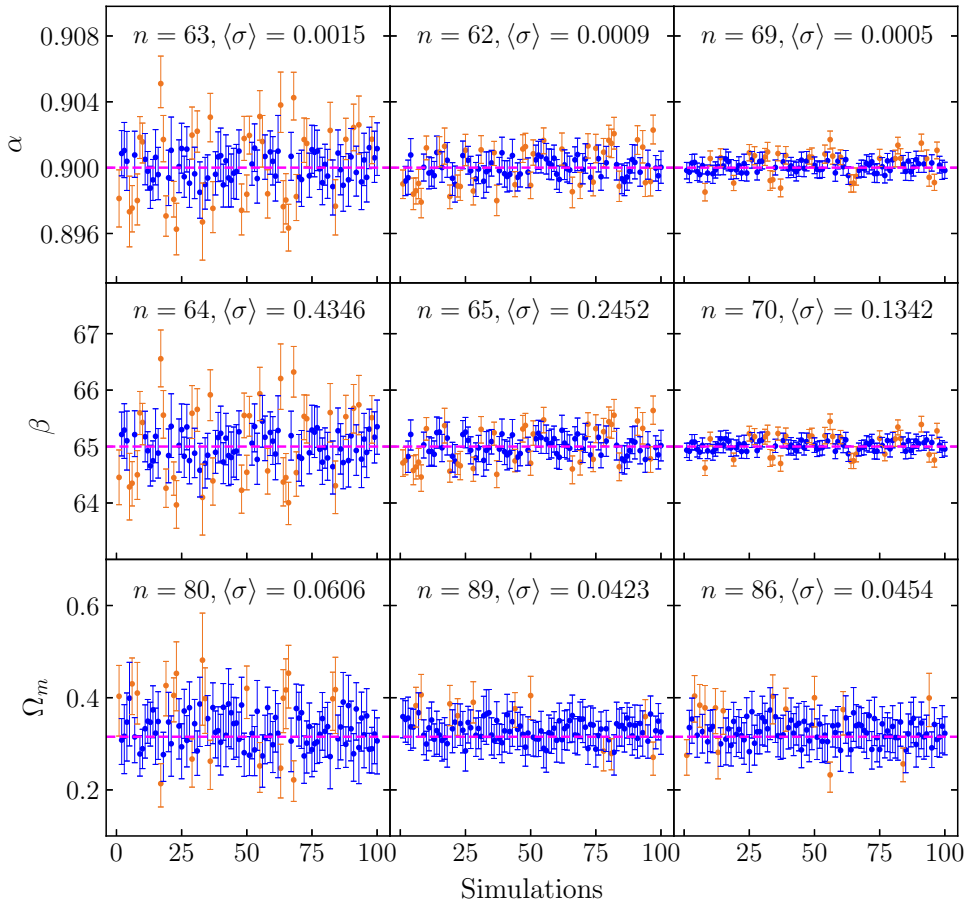


FIG. 6: The same as in Fig. 3, but for the cases of $N_{\rm FRB} = 500$ and $z_d = 0.1$ (left panels), 0.2 (middle panels) and 0.5 (right panels) type Ib FRBs, respectively. See Sec. IV D for details.

generate the mock type Ib FRBs can be found within $1\sigma$ region in most of the 100 simulations ($\sim 70\%$ for $\alpha$ and $\beta$, 86% for $\Omega_m$). This implies that the constraints from these mock type Ib FRBs are fairly reliable and robust. The pipeline of calibrating type Ib FRBs as standard candles to study cosmology works well. In the followings, we will test the key factors affecting the calibration and the cosmological constraints, by considering other cases different from the fiducial case.

### C. The number of type Ib FRBs

In the the fiducial case, we have set $N_{\rm FRB} = 500$, $z_d = 0.5$, $\sigma_{\mu,\,\rm rel} = 0.2\%$, and $\sigma_{F,\,\rm rel} = \sigma_{S,\,\rm rel} = 1\%$. Clearly, the number of type Ib FRBs (namely $N_{\rm FRB}$) plays an important role. It is easy to expect that the constraints become better for the larger $N_{\rm FRB}$. However, the time we have to wait becomes longer to accumulate a larger amount of type Ib FRBs with identified redshifts. So, the suitable question is how many type Ib FRBs with identified redshifts are enough to get the acceptable constraints?

Here, we modify the fiducial case by considering $N_{\rm FRB} = 100$, 300, and 1000, while the other settings keep unchanged. Following the similar pipeline in Sec. IV B for the fiducial case, in Fig. 4 we present the marginalized $1\sigma$ constraints on the parameters $\alpha$, $\beta$ in the empirical relation (14) and the cosmological parameter $\Omega_m$ for 100 simulations in the cases of $N_{\rm FRB} = 100$, 300, and 1000. Note that Fig. 4 should be viewed together with Fig. 3 ($N_{\rm FRB} = 500$). It is easy to see from Figs. 3 and 4 that the assumed values $\alpha = 0.9$, $\beta = 65$, and $\Omega_m = 0.3153$ used in Sec. IV A to generate the mock type Ib FRBs can be found within $1\sigma$ region in most of the 100 simulations (namely $62 \sim 71\%$ for $\alpha$ and $\beta$, $73 \sim 94\%$ for $\Omega_m$). This implies that the constraints from these mock type Ib FRBs are fairly reliable and robust. Clearly, we find from Figs. 3 and 4 that the constraints on $\alpha$, $\beta$ and $\Omega_m$ become better for larger $N_{\rm FRB}$, as expected.

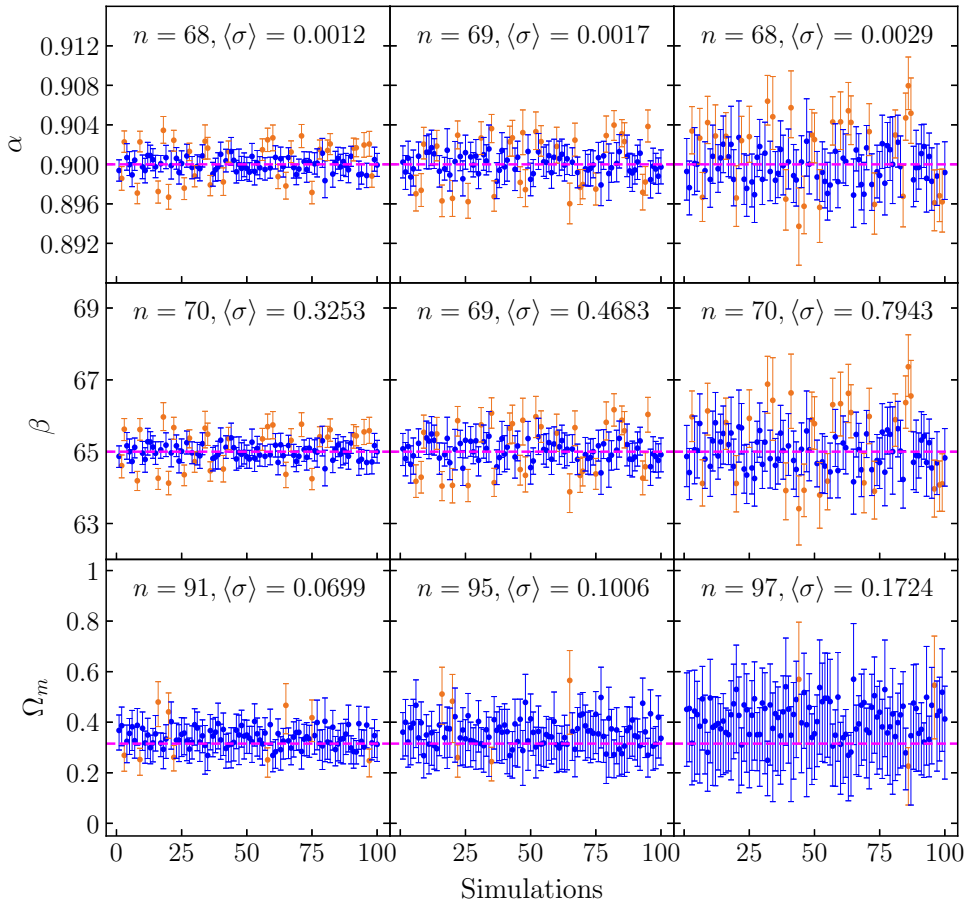


FIG. 7: The same as in Fig. 3, but for the cases of $N_{\rm FRB} = 300$, $z_d = 0.2$, and $\sigma_{\mu,\,\rm rel} = 0.2\%$ (left panels), 0.5% (middle panels), 1% (right panels), respectively. See Sec. IV E for details.

In particular, the mean of the uncertainties $\langle\sigma\rangle = 0.2090$ for $\Omega_m$ in the case of $N_{\rm FRB} = 100$ (bottom-left panel of Fig. 4) is too large ($\sim 66\%$) compared with the assumed value $\Omega_m = 0.3153$. So, $N_{\rm FRB} = 100$ is not enough to get the acceptable constraints. But the cases of $N_{\rm FRB} = 300$ and 500 are acceptable, since the uncertainties decrease dramatically. Although $N_{\rm FRB} = 1000$ is best, the cost is expensive to accumulate such a large amount of type Ib FRBs with identified redshifts. So, we only consider the cases of $N_{\rm FRB} = 300$ and 500 in the followings.

### D. The redshift divide

It is expected that the closer FRBs are easier to be detected and localized in the host galaxies. So, the lower redshift divide $z_d$ might be better. But it cannot be very low, otherwise there will be not enough type Ib FRBs at $z < z_d$ to calibrate the empirical relation (14) with an acceptable precision. We try to find a suitable redshift divide $z_d$ in the balance.

We consider the redshift divides $z_d = 0.1$, 0.2 and 0.5 for the cases of $N_{\rm FRB} = 300$ and 500, respectively, while the other settings of the fiducial case keep unchanged. Following the similar pipeline in Sec. IV B for the fiducial case, in Figs. 5 and 6 we present the marginalized $1\sigma$ constraints on the parameters $\alpha$, $\beta$ and $\Omega_m$ for 100 simulations in the cases of $N_{\rm FRB} = 300$ and 500, respectively. We find from Figs. 5 and 6 that the constraints from the mock type Ib FRBs are fairly reliable and robust, since the assumed values $\alpha = 0.9$, $\beta = 65$, and $\Omega_m = 0.3153$ used in Sec. IV A to generate the mock type Ib FRBs can be found within $1\sigma$ region in most of the 100 simulations (namely $62 \sim 70\%$ for $\alpha$ and $\beta$, $80 \sim 93\%$ for $\Omega_m$). From Figs. 5 and 6, it is easy to see that the uncertainties $\langle\sigma\rangle$ for $\alpha$, $\beta$ and $\Omega_m$ in the cases of $z_d = 0.1$ are all much larger than (about 2 times of) the ones in the cases of $z_d = 0.2$ and 0.5. Thus, $z_d = 0.1$ is

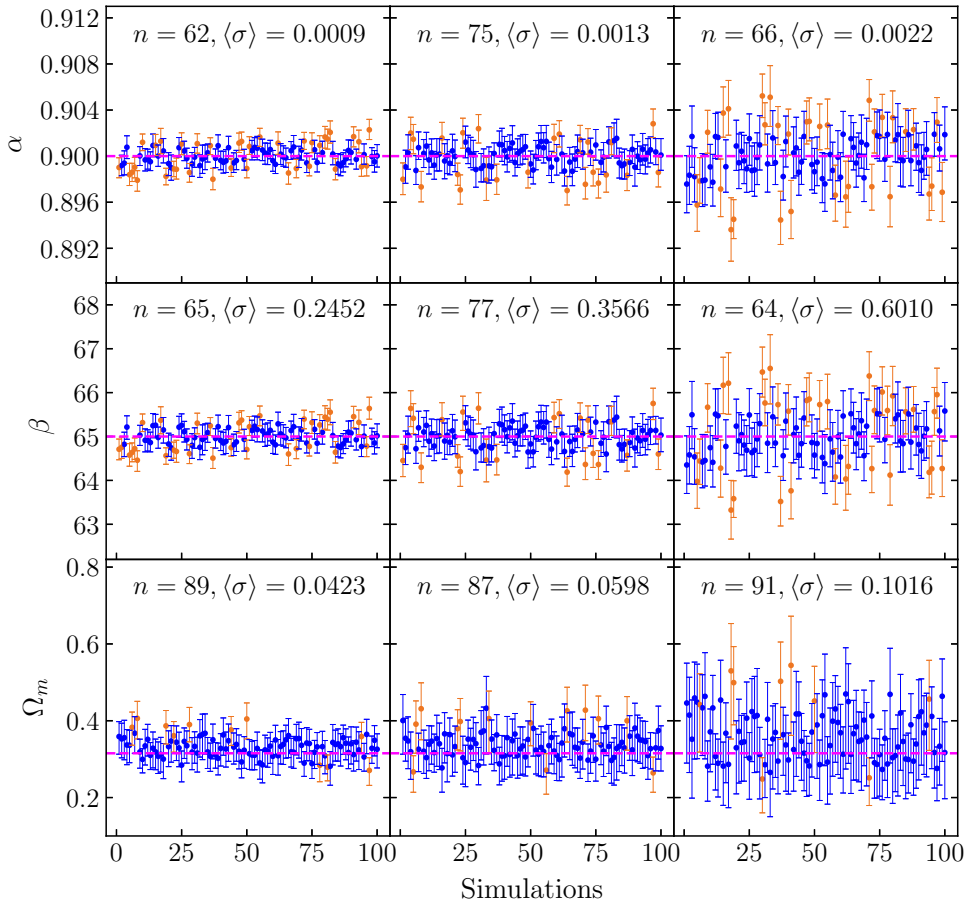


FIG. 8: The same as in Fig. 3, but for the cases of $N_{\rm FRB} = 500$, $z_d = 0.2$, and $\sigma_{\mu,\,\rm rel} = 0.2\%$ (left panels), 0.5% (middle panels), 1% (right panels), respectively. See Sec. IV E for details.

not suitable. Although the constraints on $\alpha$ and $\beta$ in the cases of $z_d = 0.5$ are better than the ones in the cases of $z_d = 0.2$, the constraints on the cosmological parameter $\Omega_m$ are at the same level in both cases of $z_d = 0.5$ and 0.2. In this sense, we prefer $z_d = 0.2$ to 0.5 since a lower redshift divide is easier to achieve, as mentioned above. The number of type Ib FRBs ($N_{\rm FRB} = 300$ or 500) makes almost no difference at this point. So, we consider that $z_d = 0.2$ might be a suitable choice on balance.

### E. The precision of the distance modulus

In the fiducial case, we have assumed that the distance modulus $\mu$ can be measured with high precision, namely the relative error $\sigma_{\mu,\,\rm rel} = 0.2\%$ [50] in the era of the Roman Space Telescope (formerly WFIRST). But before the launch of the Roman Space Telescope, how does this precision affect the calibration and the cosmological constraints?

We consider the relative error $\sigma_{\mu,\,\rm rel} = 0.2\%$, 0.5% and 1% for the cases of $N_{\rm FRB} = 300$ and 500, respectively, while $z_d = 0.2$ and $\sigma_{F,\,\rm rel} = \sigma_{S,\,\rm rel} = 1\%$ (as in the fiducial case). Again, in Figs. 7 and 8 we present the marginalized $1\sigma$ constraints on the parameters $\alpha$, $\beta$ and $\Omega_m$ for 100 simulations in the cases of $N_{\rm FRB} = 300$ and 500, respectively. We find from Figs. 7 and 8 that the constraints from the mock type Ib FRBs are fairly reliable and robust, since the assumed values $\alpha = 0.9$, $\beta = 65$, and $\Omega_m = 0.3153$ used in Sec. IV A to generate the mock type Ib FRBs can be found within $1\sigma$ region in most of the 100 simulations (namely $62 \sim 77\%$ for $\alpha$ and $\beta$, $87 \sim 97\%$ for $\Omega_m$). From Figs. 7 and 8, it is easy to see that the constraints on $\alpha$, $\beta$ and $\Omega_m$ become worse for larger $\sigma_{\mu,\,\rm rel}$. The number of type Ib FRBs ($N_{\rm FRB} = 300$ or 500) makes almost no difference at this point. In particular, the mean of the uncertainties $\langle\sigma\rangle = 0.1724$ for $\Omega_m$ in the case of $N_{\rm FRB} = 300$ and $\sigma_{\mu,\,\rm rel} = 1\%$ (bottom-right panel of Fig. 7) is too

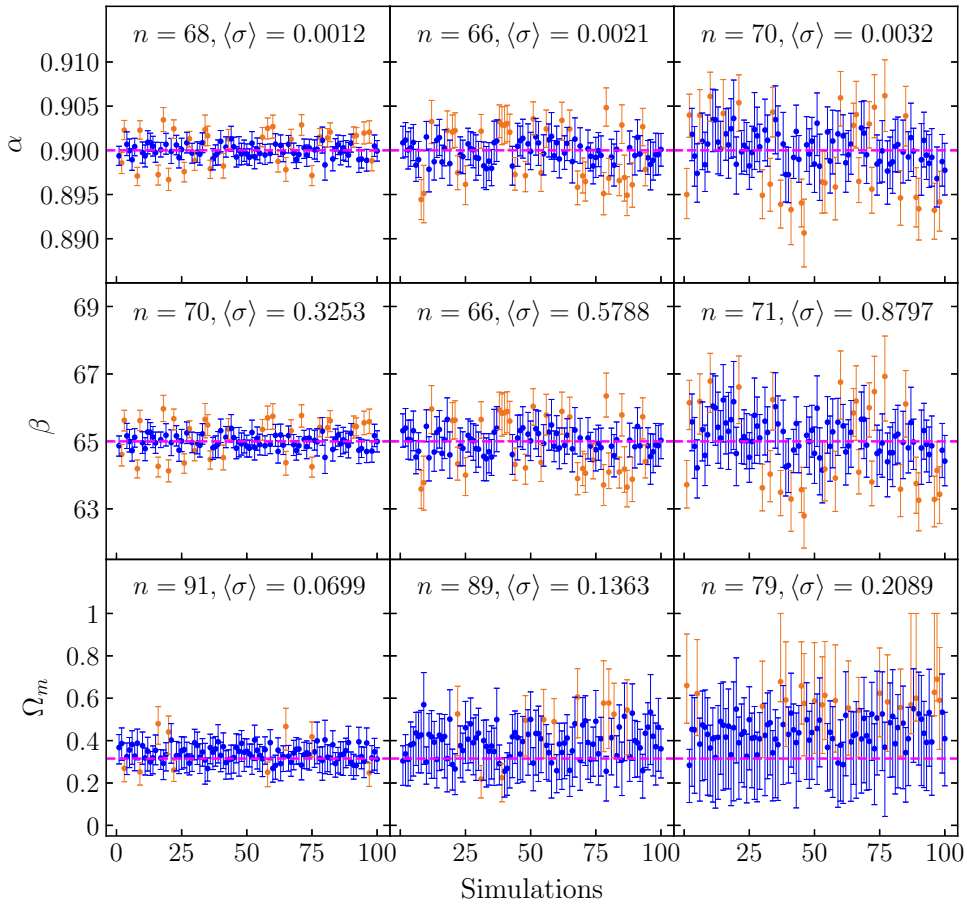


FIG. 9: The same as in Fig. 3, but for the cases of $N_{\rm FRB} = 300$, $z_d = 0.2$, $\sigma_{\mu,\,\rm rel} = 0.2\%$, and $\sigma_{F,\,\rm rel} = \sigma_{S,\,\rm rel} = 1\%$ (left panels), 2% (middle panels), 3% (right panels), respectively. See Sec. IV F for details.

large ($\sim 55\%$) compared with the assumed value $\Omega_m = 0.3153$. But it can decrease to $\langle\sigma\rangle = 0.1016$ at the price of increasing the number of type Ib FRBs to $N_{\rm FRB} = 500$ (bottom-right panel of Fig. 8). The case of $\sigma_{\mu,\,\rm rel} = 0.2\%$ is best, while the case of $\sigma_{\mu,\,\rm rel} = 0.5\%$ is also acceptable, regardless of $N_{\rm FRB} = 300$ or 500. Note that currently SNIa can be measured with the precision around 0.6% (see e.g. Union2.1 [53], Pantheon [54] and Pantheon+ [55, 56] SNIa samples). Thus, it is reasonable to expect $\sigma_{\mu,\,\rm rel} \leq 0.5\%$ in the near future for type Ib FRBs which share the same host galaxies with SNIa. On the other hand, if the Roman Space Telescope (formerly WFIRST) could be launched in mid-2020s (2025) as planed, $\sigma_{\mu,\,\rm rel} = 0.2\%$ [50] will be easily achieved very soon.

### F. The precisions of the fluence and the flux

In the fiducial case, we have assumed that the fluence $F_\nu$ and the flux $S_\nu$ could be measured with high precisions, namely the relative errors $\sigma_{F,\,\rm rel} = \sigma_{S,\,\rm rel} = 1\%$. Of course, such high precisions cannot be achieved currently in the actual data of FRBs. Since FRBs have become a very promising and thriving field in astronomy and cosmology recently, many observational efforts have been dedicated to FRBs, and hence it is reasonable to expect some breakthroughs in the observations and the instruments in the future. Thus, it is of interest to see the effects of these precisions on the calibration of type Ib FRBs and their cosmological constraints.

We consider the relative errors $\sigma_{F,\,\rm rel} = \sigma_{S,\,\rm rel} = 1\%$, 2% and 3% for the cases of $N_{\rm FRB} = 300$ and 500, respectively, while $z_d = 0.2$ and $\sigma_{\mu,\,\rm rel} = 0.2\%$ (as in the fiducial case). Similarly, we present the results in Figs. 9 and 10. We find from Figs. 9 and 10 that the constraints from the mock type Ib FRBs are fairly reliable and robust, since the assumed values $\alpha = 0.9$, $\beta = 65$, and $\Omega_m = 0.3153$ used in Sec. IV A to

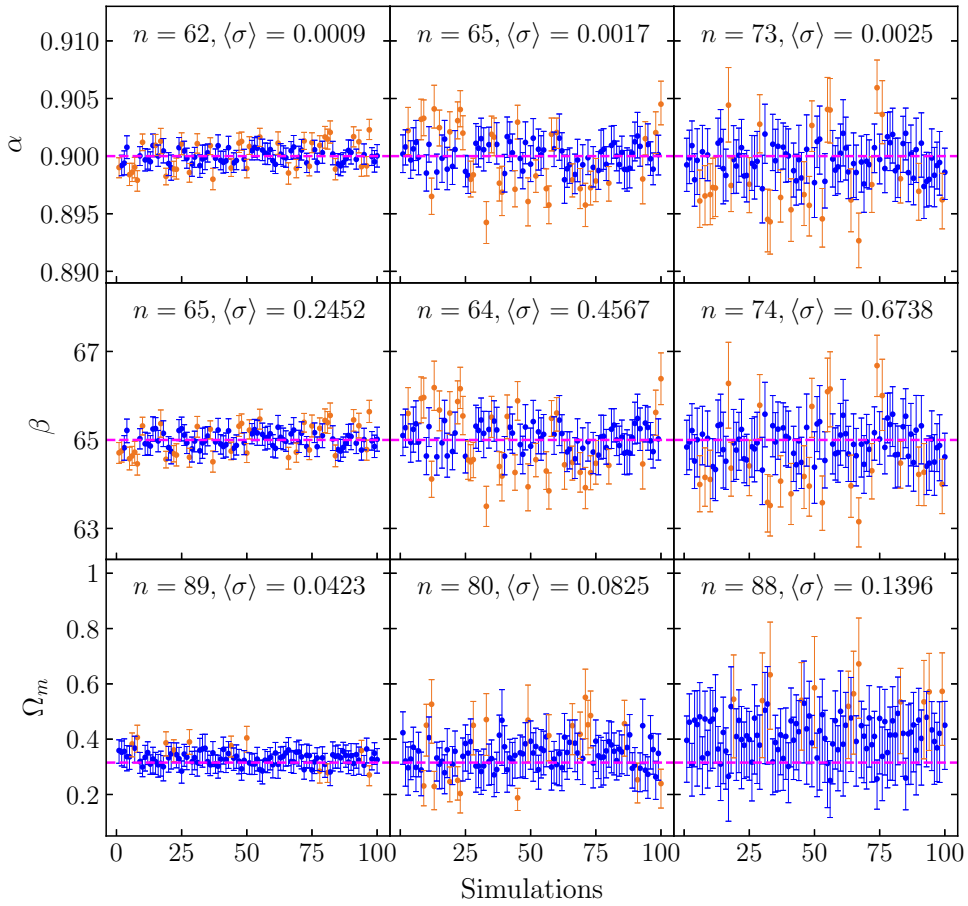


FIG. 10: The same as in Fig. 3, but for the cases of $N_{\rm FRB} = 500$, $z_d = 0.2$, $\sigma_{\mu,\,\rm rel} = 0.2\%$, and $\sigma_{F,\,\rm rel} = \sigma_{S,\,\rm rel} = 1\%$ (left panels), 2% (middle panels), 3% (right panels), respectively. See Sec. IV F for details.

generate the mock type Ib FRBs can be found within $1\sigma$ region in most of the 100 simulations (namely $62 \sim 74\%$ for $\alpha$ and $\beta$, $79 \sim 91\%$ for $\Omega_m$). From Figs. 9 and 10, it is easy to see that the constraints on $\alpha$, $\beta$ and $\Omega_m$ become worse for larger $\sigma_{F,\,\rm rel} = \sigma_{S,\,\rm rel}$. The number of type Ib FRBs ($N_{\rm FRB} = 300$ or 500) makes almost no difference at this point. In particular, the mean of the uncertainties $\langle\sigma\rangle = 0.2089$ for $\Omega_m$ in the case of $N_{\rm FRB} = 300$ and $\sigma_{F,\,\rm rel} = \sigma_{S,\,\rm rel} = 3\%$ (bottom-right panel of Fig. 9) is too large ($\sim 66\%$) compared with the assumed value $\Omega_m = 0.3153$. Although it can decrease to $\langle\sigma\rangle = 0.1396$ at the price of increasing the number of type Ib FRBs to $N_{\rm FRB} = 500$ (bottom-right panel of Fig. 10), this is still unacceptable since $0.1396/0.3153 \simeq 44\%$. In this sense, the case of $\sigma_{F,\,\rm rel} = \sigma_{S,\,\rm rel} = 3\%$ is not enough to get the acceptable constraints on the cosmological models. One of the ways out is to significantly increase the number of type Ib FRBs (say, $N_{\rm FRB} = 1000$ or even more). On the other hand, the cases of $\sigma_{F,\,\rm rel} = \sigma_{S,\,\rm rel} = 1\%$ and 2% are acceptable. Anyway, improving the precisions of the fluences and the fluxes for FRBs is an important task in the future.

### G. Three-parameter empirical relation

In the above discussions, the empirical relation given in Eq. (14) is considered. This is a two-parameter empirical relation, with $\alpha$ and $\beta$ as the free parameters. The coefficients for the terms of $\log F_\nu$ and $\log S_\nu$ are not independent. The cause roots in the empirical $L_\nu - E$ relation given in Eq. (13) due to the unknown physical mechanism for the engines of type Ib FRBs.

However, if one pretends to do not know the empirical $L_\nu - E$ relation given in Eq. (13), the empirical relation between the distance modulus $\mu$ (equivalently the luminosity distance $d_L$), the fluence $F_\nu$ and the flux $S_\nu$ could be instead regarded as a three-parameter empirical relation without any underlying

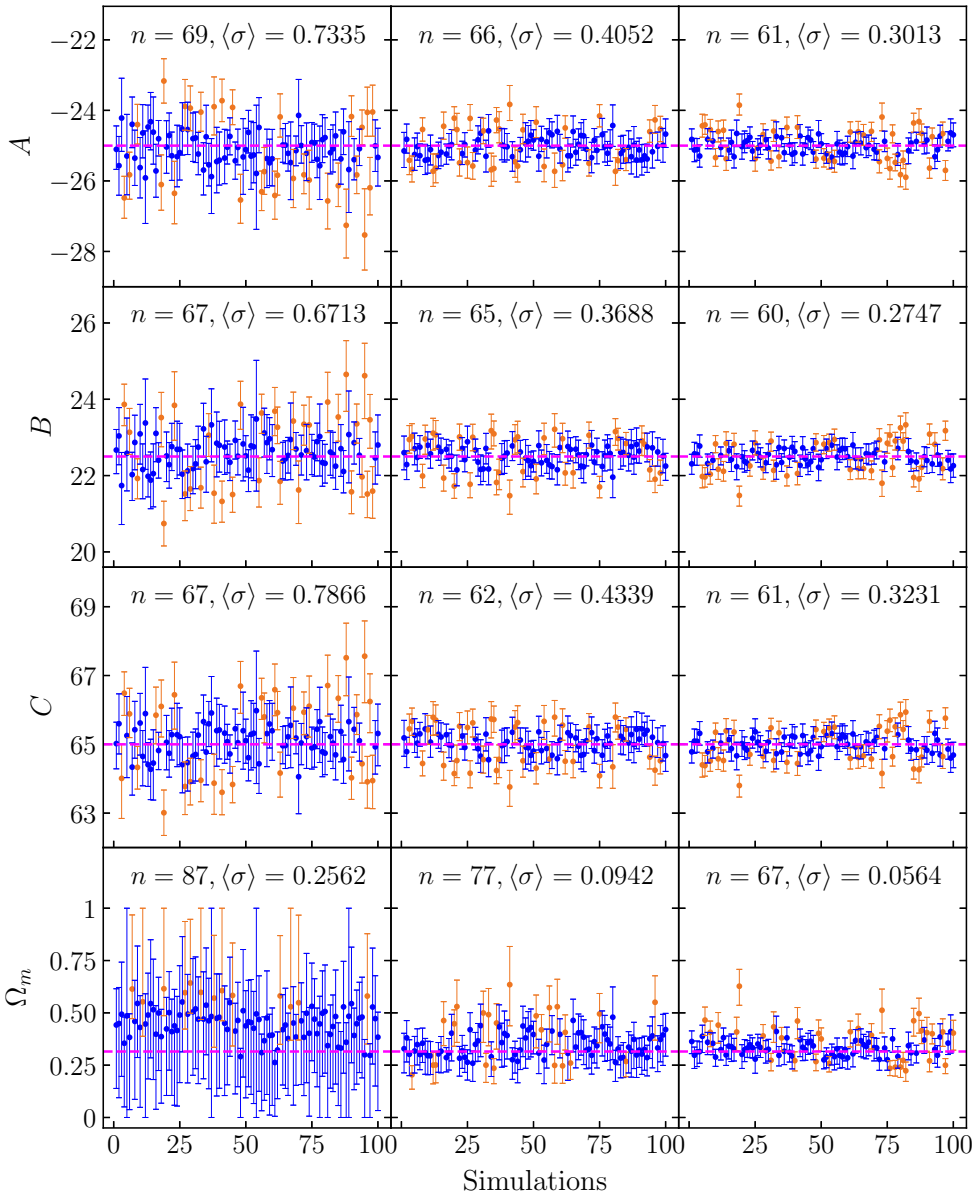


FIG. 11: The same as in Fig. 3, but for the case of three-parameter empirical relation with $N_{\rm FRB} = 100$ (left panels), 300 (middle panels) and 500 (right panels). See Sec. IV G for details.

physical mechanism for the engines of type Ib FRBs, namely

$$\mu = A \log \frac{F_\nu/(1+z)}{\rm Jy\ ms} + B \log \frac{S_\nu}{\rm Jy} + C\,, \tag{23}$$

where the independent parameters $A$, $B$ and $C$ are all dimensionless constants. The assumed underlying empirical relation given by Eq. (20) used in Sec. IV A to generate the mock type Ib FRBs corresponds to $A = -25$, $B = 22.5$ and $C = 65$. One can calibrate the three-parameter empirical relation (23) by using type Ib FRBs at low redshifts $z < z_d$, and then obtain the distance moduli $\mu$ for type Ib FRBs at high redshifts $z \geq z_d$ by using this calibrated three-parameter empirical relation. Thus, one can constrain the cosmological models with these type Ib FRBs at high redshifts $z \geq z_d$.

We consider the cases of $N_{\rm FRB} = 100$, 300 and 500 with $z_d = 0.2$, $\sigma_{\mu,\,\rm rel} = 0.2\%$, and $\sigma_{F,\,\rm rel} = \sigma_{S,\,\rm rel} = 1\%$ (as in the fiducial case). In Fig. 11, we present the marginalized $1\sigma$ constraints on the parameters $A$, $B$, $C$ and $\Omega_m$ for 100 simulations in the cases of $N_{\rm FRB} = 100$, 300 and 500, respectively. We find

from Fig. 11 that the constraints from the mock type Ib FRBs are fairly reliable and robust, since the assumed values $A = -25$, $B = 22.5$, $C = 65$, and $\Omega_m = 0.3153$ used in Sec. IV A to generate the mock type Ib FRBs can be found within $1\sigma$ region in most of the 100 simulations (namely $60 \sim 69\%$ for $A$, $B$ and $C$, $67 \sim 87\%$ for $\Omega_m$). Comparing Fig. 11 with the cases of two-parameter empirical relation, the uncertainties $\langle\sigma\rangle$ become larger. This is not surprising, since the number of independent parameters has been increased. On the other hand, the mean of the uncertainties $\langle\sigma\rangle = 0.2562$ for $\Omega_m$ in the case of $N_{\rm FRB} = 100$ (bottom-left panel of Fig. 11) is too large ($\sim 81\%$) compared with the assumed value $\Omega_m = 0.3153$. Thus, $N_{\rm FRB} = 100$ is not enough to get the acceptable constraints. But the uncertainties dramatically decrease in the cases of $N_{\rm FRB} = 300$ and 500, and hence they are acceptable. Comparing with the middle panels of Fig. 5 ($N_{\rm FRB} = 300$) and Fig. 6 ($N_{\rm FRB} = 500$) in the case of two-parameter empirical relation, we find that the constraints on the cosmological parameter $\Omega_m$ become looser in the case of three-parameter empirical relation. So, we consider that the two-parameter empirical relation (14) should be preferred in the FRB cosmology.

## V. CONCLUDING REMARKS

Recently, FRBs have become a thriving field in astronomy and cosmology. Due to their extragalactic and cosmological origin, they are useful to study the cosmic expansion and IGM. In the literature, the dispersion measure DM of FRB has been considered extensively. It could be used as an indirect proxy of the luminosity distance $d_L$ of FRB. The observed DM contains the contributions from the Milky Way (MW), the MW halo, IGM, and the host galaxy. Unfortunately, IGM and the host galaxy of FRB are poorly known to date, and hence the large uncertainties of $\rm DM_{IGM}$ and $\rm DM_{host}$ in DM plague the FRB cosmology. Could we avoid DM in studying cosmology? Could we instead consider the luminosity distance $d_L$ directly in the FRB cosmology? We are interested to find a way out for this problem in the present work. From the lessons of calibrating SNIa or long GRBs as standard candles, we consider a universal subclassification scheme for FRBs, and there are some empirical relations for them. In the present work, we propose to calibrate type Ib FRBs as standard candles by using a tight empirical relation without DM. The calibrated type Ib FRBs at high redshifts can be used like SNIa to constrain the cosmological models. We also test the key factors affecting the calibration and the cosmological constraints.

We find that the constraints become better for the larger number of type Ib FRBs. $N_{\rm FRB} = 100$ is not enough to get the acceptable constraints, while $N_{\rm FRB} = 300$ or 500 are suitable. We also find that the redshift divide $z_d = 0.1$ is not suitable, and we suggest that $z_d = 0.2$ might be a suitable choice on balance. It is found that the precision of the distance modulus $\sigma_{\mu,\,\rm rel} \leq 0.5\%$ is enough to get the acceptable constraints, which can be achieved very soon. On the other hand, the precisions of the fluence and the flux $\sigma_{F,\,\rm rel} = \sigma_{S,\,\rm rel} \geq 3\%$ is not enough to get the acceptable constraints on the cosmological models. One of the ways out is to significantly increase the number of type Ib FRBs (say, $N_{\rm FRB} = 1000$ or even more). Anyway, improving the precisions of the fluences and the fluxes for FRBs is an important task in the future. Although one could instead consider a three-parameter empirical relation (23), we suggest that the two-parameter empirical relation (14) should be preferred in the FRB cosmology.

Of course, current data of FRBs are certainly not enough to calibrate type Ib FRBs as standard candles. So, it is a proof of concept by using the simulated FRBs in the present work. But the same pipeline holds for the actual type Ib FRBs in the future. Since FRBs have become a very promising and thriving field in astronomy and cosmology recently, many observational efforts have been dedicated to FRBs, and hence it is reasonable to expect some breakthroughs in the observations and the instruments in the future. Let us be optimistic with the hope to actually use type Ib FRBs as standard candles.

Clearly, the key to calibrate type Ib FRBs as standard candles is that there is really a tight empirical relation for them, due to the unknown physical mechanism for the engines of type Ib FRBs. The universal subclassification scheme for FRBs proposed in [16] and the empirical relations found in [16] should be carefully examined by using the larger and better FRB datasets in the future. On the other hand, the theories that could produce such an empirical relation for type Ib FRBs are desirable.

As mentioned in [16], there might be three methods to identify type Ib FRBs: (a) their distribution tracks SFH. But this does not work for an individual FRB. (b) the physical criteria similar to the ones given by Eqs. (4) and (5). (c) the precise localizations of FRBs. We prefer the last method in practice. If a non-repeating (type I) FRB has been precisely localized by using e.g. VLBI down to the milliarcsecond

level [44, 45] or better in the future, its host galaxy and local environment can be well determined. Subsequently, it is a type Ib FRB if this FRB lives in a star-forming environment. Of course, its redshift can also be identified accordingly in this way.

Note that in the present work we constrain the cosmological model by using the calibrated type Ib FRBs at high redshifts alone. But this is not necessary. In fact, similar to the case of SNIa, it is better to combine them with other observations (e.g. cosmic microwave background (CMB) and large-scale structure) to obtain the much tighter cosmological constraints.

## ACKNOWLEDGEMENTS

We are grateful to Da-Chun Qiang, Hua-Kai Deng, Shupeng Song, Jing-Yi Jia and Shu-Ling Li for kind help and useful discussions. This work was supported in part by NSFC under Grants No. 11975046 and No. 11575022.

[1] https://www.nature.com/collections/rswtktxcln
[2] D. R. Lorimer, Nat. Astron. **2**, 860 (2018) [arXiv:1811.00195].
[3] E. F. Keane, Nat. Astron. **2**, 865 (2018) [arXiv:1811.00899].
[4] E. Petroff, J. W. T. Hessels and D. R. Lorimer, Astron. Astrophys. Rev. **30**, 2 (2022) [arXiv:2107.10113].
[5] B. Zhang, arXiv:2212.03972 [astro-ph.HE].
[6] B. Zhang, Nature **587**, 45 (2020) [arXiv:2011.03500].
[7] D. Xiao, F. Y. Wang and Z. G. Dai, Sci. China Phys. Mech. Astron. **64**, 249501 (2021) [arXiv:2101.04907].
[8] W. Deng and B. Zhang, Astrophys. J. **783**, L35 (2014) [arXiv:1401.0059].
[9] Y. P. Yang and B. Zhang, Astrophys. J. **830**, no. 2, L31 (2016) [arXiv:1608.08154].
[10] H. Gao, Z. Li and B. Zhang, Astrophys. J. **788**, 189 (2014) [arXiv:1402.2498].
[11] B. Zhou, X. Li, T. Wang, Y. Z. Fan and D. M. Wei, Phys. Rev. D **89**, 107303 (2014) [arXiv:1401.2927].
[12] D. C. Qiang, H. K. Deng and H. Wei, Class. Quant. Grav. **37**, 185022 (2020) [arXiv:1902.03580].
[13] D. C. Qiang and H. Wei, JCAP **2004**, 023 (2020) [arXiv:2002.10189].
[14] D. C. Qiang and H. Wei, Phys. Rev. D **103**, 083536 (2021) [arXiv:2102.00579].
[15] D. C. Qiang, S. L. Li and H. Wei, JCAP **2201**, 040 (2022) [arXiv:2111.07476].
[16] H. Y. Guo and H. Wei, JCAP **2207**, 010 (2022) [arXiv:2203.12551].
[17] M. McQuinn, Astrophys. J. **780**, L33 (2014) [arXiv:1309.4451].
[18] K. Ioka, Astrophys. J. **598**, L79 (2003) [astro-ph/0309200].
[19] S. Inoue, Mon. Not. Roy. Astron. Soc. **348**, 999 (2004) [astro-ph/0309364].
[20] M. Jaroszynski, Mon. Not. Roy. Astron. Soc. **484**, no. 2, 1637 (2019) [arXiv:1812.11936].
[21] H. S. Leavitt and E. C. Pickering, Harvard College Observatory Circular, **173**, 1 (1912).
[22] M. M. Phillips, Astrophys. J. Lett. **413**, L105 (1993).
[23] A. G. Riess *et al.*, Astrophys. J. Lett. **934**, no.1, L7 (2022) [arXiv:2112.04510].
[24] N. Liang, W. K. Xiao, Y. Liu and S. N. Zhang, Astrophys. J. **685**, 354 (2008) [arXiv:0802.4262].
[25] H. Wei, JCAP **1008**, 020 (2010) [arXiv:1004.4951].
[26] L. Amati *et al.*, Astron. Astrophys. **390**, 81 (2002) [astro-ph/0205230].
[27] B. E. Schaefer, Astrophys. J. **660**, 16 (2007) [astro-ph/0612285].
[28] H. Wei and S. N. Zhang, Eur. Phys. J. C **63**, 139-147 (2009) [arXiv:0808.2240].
[29] J. Liu and H. Wei, Gen. Rel. Grav. **47**, no.11, 141 (2015) [arXiv:1410.3960].
[30] B. C. Andersen *et al.*, Nature **587**, no. 7832, 54 (2020) [arXiv:2005.10324].
[31] C. D. Bochenek *et al.*, Nature **587**, no. 7832, 59 (2020) [arXiv:2005.10828].
[32] L. Lin *et al.*, Nature **587**, no. 7832, 63 (2020) [arXiv:2005.11479].
[33] C. K. Li *et al.*, Nat. Astron. **5**, 378 (2021) [arXiv:2005.11071].
[34] S. P. Tendulkar *et al.*, Astrophys. J. Lett. **834**, no.2, L7 (2017) [arXiv:1701.01100].
[35] B. Marcote *et al.*, Nature **577**, no.7789, 190 (2020) [arXiv:2001.02222].
[36] C. H. Niu *et al.*, Nature **606**, no.7916, 873 (2022) [arXiv:2110.07418].
[37] M. Bhardwaj *et al.*, Astrophys. J. Lett. **919**, no.2, L24 (2021) [arXiv:2108.12122].

[38] M. Bhardwaj *et al.*, Astrophys. J. Lett. **910**, no.2, L18 (2021) [arXiv:2103.01295].
[39] F. Kirsten *et al.*, Nature **602**, no.7898, 585 (2022) [arXiv:2105.11445].
[40] K. Nimmo *et al.*, Nat. Astron. **6**, 393 (2022) [arXiv:2105.11446].
[41] R. C. Zhang and B. Zhang, Astrophys. J. Lett. **924**, no.1, L14 (2022) [arXiv:2109.07558].
[42] M. Amiri *et al.*, Astrophys. J. Supp. **257**, no.2, 59 (2021) [arXiv:2106.04352].
The data for CHIME/FRB Catalog 1 in machine-readable format can be found via their public webpage at https://www.chime-frb.ca/catalog
[43] R. C. Zhang *et al.*, Mon. Not. Roy. Astron. Soc. **501**, no.1, 157 (2021) [arXiv:2011.06151].
[44] B. Marcote *et al.*, PoS **EVN2021**, 035 (2021) [arXiv:2202.11644].
[45] B. Marcote and Z. Paragi, PoS **EVN2018**, 013 (2019) [arXiv:1901.08541].
[46] B. Zhang, Astrophys. J. Lett. **867**, no.2, L21 (2018) [arXiv:1808.05277].
[47] K. E. Heintz *et al.*, Astrophys. J. **903**, 152 (2020) [arXiv:2009.10747].
The up-to-date compilation of all known FRB host galaxies is available at https://frbhosts.org
[48] N. Aghanim *et al.*, Astron. Astrophys. **641**, A6 (2020) [arXiv:1807.06209].
[49] P. Madau and T. Fragos, Astrophys. J. **840**, no.1, 39 (2017) [arXiv:1606.07887].
[50] D. Spergel *et al.*, arXiv:1305.5425 [astro-ph.IM].
[51] J. Torrado and A. Lewis, JCAP **2105**, 057 (2021) [arXiv:2005.05290],
available at https://cobaya.readthedocs.org
[52] A. Lewis and S. Bridle, Phys. Rev. D **66**, 103511 (2002) [astro-ph/0205436],
available at https://cosmologist.info/cosmomc/
[53] N. Suzuki *et al.*,, Astrophys. J. **746**, 85 (2012) [arXiv:1105.3470].
[54] D. M. Scolnic *et al.*, Astrophys. J. **859**, no.2, 101 (2018) [arXiv:1710.00845].
[55] D. Scolnic *et al.*, Astrophys. J. **938**, no.2, 113 (2022) [arXiv:2112.03863].
[56] D. Brout *et al.*, Astrophys. J. **938**, no.2, 110 (2022) [arXiv:2202.04077].